ARTICLES
PUBLISHED ONLINE: 20 JULY 2014 | DOI: 10.1038/NMAT4035
nature materials

Separation of rare gases and chiral molecules by selective binding in porous organic cages

Linjiang Chen[1], Paul S. Reiss[1], Samantha Y. Chong[1], Daniel Holden[1], Kim E. Jelfs[1], Tom Hasell[1], Marc A. Little[1], Adam Kewley[1], Michael E. Briggs[1], Andrew Stephenson[1], K. Mark Thomas[2], Jayne A. Armstrong[2], Jon Bell[2], Jose Busto[3], Raymond Noel[3], Jian Liu[4], Denis M. Strachan[4], Praveen K. Thallapally[4] and Andrew I. Cooper[1]*

The separation of molecules with similar size and shape is an important technological challenge. For example, rare gases can pose either an economic opportunity or an environmental hazard and there is a need to separate these spherical molecules selectively at low concentrations in air. Likewise, chiral molecules are important building blocks for pharmaceuticals, but chiral enantiomers, by definition, have identical size and shape, and their separation can be challenging. Here we show that a porous organic cage molecule has unprecedented performance in the solid state for the separation of rare gases, such as krypton and xenon. The selectivity arises from a precise size match between the rare gas and the organic cage cavity, as predicted by molecular simulations. Breakthrough experiments demonstrate real practical potential for the separation of krypton, xenon and radon from air at concentrations of only a few parts per million. We also demonstrate selective binding of chiral organic molecules such as 1-phenylethanol, suggesting applications in enantioselective separation.

With the exception of argon, which makes up almost 1% of air, the rare or 'noble' gases are all commonly encountered in low concentrations: xenon (Xe) occurs naturally in the atmosphere at 0.087 parts per million by volume (ppmv); krypton (Kr) at 1.14 ppmv (ref. 1). Cryogenic methods are used to extract commercially valuable rare gases such as xenon from air, but this is costly because of the low concentrations involved. Rare gases are therefore valuable: high-purity xenon, for example, has uses including commercial lighting, medical imaging, anaesthesia and neuroprotection, and it sells for more than $\$5{,}000\ kg^{-1}$.

Other rare gas isotopes can be harmful. Radon gas, which occurs naturally in a radioactive form (^{222}Rn), can accumulate in buildings, and is a leading cause of lung cancer[2], accounting for around 21,000 deaths per year in the USA alone. Likewise, unstable, hazardous radioisotopes of krypton and xenon, such as ^{85}Kr and ^{133}Xe, are produced in nuclear fission and can enter the atmosphere during the reprocessing of spent nuclear fuel[3] or via nuclear accidents, such as the Fukushima Daiichi nuclear power plant catastrophe in Japan[4]. Cryogenic processes have been suggested for the removal of radioactive rare gases from off-gas streams in future nuclear reprocessing plants, but again this is energy intensive and expensive because of the low rare gas concentrations. Alternative separation technologies therefore could save energy, protect the environment, and produce valuable resources: for example, the reduction of ^{85}Kr concentrations to permissible levels in xenon-rich nuclear reprocessing streams would create an entirely new source of xenon for industrial use.

In principle, gas mixtures can be separated with greater energy efficiency by using porous solids that bind specific components in the mixture, as suggested by early experiments on the adsorption of 'radium emanations' (radon) on charcoal by Rutherford[5]. A wide range of task-specific porous materials now exists, such as activated carbons[6,7], zeolites[8], metal–organic frameworks (MOFs; refs 9,10), porous molecular crystals[11], and polymers[12]. It remains a major challenge, however, to efficiently separate gas molecules that are present in low concentrations (<500 ppmv) from the principal components in the gas mixture. For rare gases, this is exacerbated by their lack of chemical reactivity and the small size difference between the higher-mass rare gases, such as Kr (diameter = 3.69 Å; ref. 13), Xe (4.10 Å) and Rn (4.17 Å), and the common constituents of air. The spherical nature of the rare gases precludes strategies based on shape selectivity[14]; hence precise tuning of the dimensions of the pores is required to achieve selective separations. Ideally, an adsorbent should exhibit both high adsorption selectivity and high adsorption capacity for the component of interest. The provision of a large physical surface area may not give good separation selectivity, but adequate adsorption capacity is nonetheless required to create economically viable separation methods.

Porous MOFs show promise for Xe/Kr separations[15–17] and computational screening studies suggest that better materials remain to be discovered[13,18]. Few materials, however, provide effective separations of rare gases at low concentrations of just a few parts per million in air. The leading material is the nickel-based MOF, Ni/DOBDC, which was shown to separate 400 ppm Xe from 40 ppm Kr in air containing O_2, N_2 and CO_2 with a Xe/Kr selectivity of 7.3 (ref. 19).

We reported previously an organic cage molecule, **CC3** (ref. 20), which we show here to have an internal cavity that is precisely the right size to accommodate a single xenon or radon atom. The largest inclusion sphere[21] in this cavity ($d = 4.4$ Å) is very close to the diameters of xenon (4.10 Å; Fig. 1c) and radon (4.17 Å). The cage packs in the crystalline state to give a robust 3D pore structure

[1]Department of Chemistry and Centre for Materials Discovery, University of Liverpool, Crown Street, Liverpool L69 7ZD, UK, [2]Wolfson Northern Carbon Reduction Laboratories, Drummond Building, Newcastle University, Newcastle upon Tyne NE1 7RU, UK, [3]CPPM, Aix-Marseille Université, CNRS/IN2P3, 163 avenue de Luminy, case 902, 13009 Marseille, France, [4]Pacific Northwest National Laboratory, Richland, Washington 99352, USA.
*e-mail: aicooper@liv.ac.uk

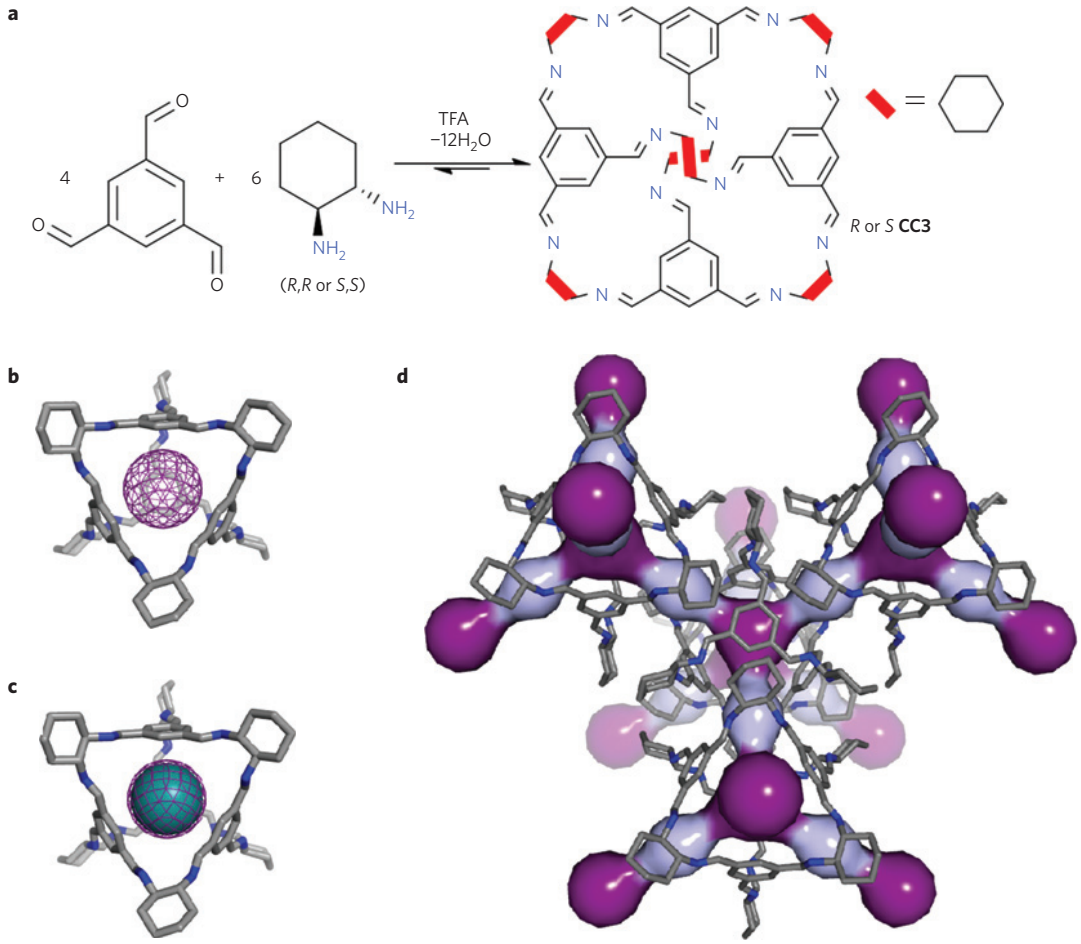

Figure 1 | The porous organic cage molecule and its extended crystal packing. a, Reaction scheme for the synthesis of **CC3** by a one-pot [4+6] cycloimination reaction involving four trialdehyde and six diamine molecules, catalysed by trifluoroacetic acid (TFA). **b**, The largest inclusion sphere inside the cage (dark purple mesh, **b**) is the perfect size to accommodate a single xenon atom (cyan sphere, **c**) or radon atom (not shown). **d**, Two pore cavities exist in the 3D pore structure: a cage cavity inside the molecule itself (dark purple) and a window cavity between adjacent cage windows (light purple).

(Fig. 1d). In a static view, however, the narrowest point in the pore channels, the pore-limiting diameter[22], lies between the cage and the window cavities and has dimensions of just 3.6 Å (vertical solid line in Fig. 2a). This is slightly smaller than the diameter of Kr (3.69 Å), and in principle too narrow to permit the diffusion of either xenon or radon. However, molecular dynamics simulations allow for vibrational motion of the atoms in the cage molecules. This reveals a time-averaged, pore-limiting envelope (Fig. 2a) that is broad enough to permit diffusion of both xenon and radon. Calculations suggest that the pore windows are 'open' for only 7% and 3% of the simulation time for xenon and radon, respectively, but this is enough to allow opportunistic hopping of these gases through the pores.

Both simulated and experimental gas adsorption isotherms demonstrate substantial uptake of both krypton and xenon in **CC3** (Fig. 2c). We also simulated the radon adsorption isotherm, which we could not measure experimentally because, to our knowledge, no laboratory worldwide is equipped with a suitable gas sorption apparatus that is configured for such radioisotopes. The xenon isotherm and the simulated radon isotherm both approach saturation at 1 bar (298 K) at a gas uptake of approximately 2.69 mol kg^{-1}, corresponding to three gas molecules per **CC3** cage. This can be rationalized by one gas molecule occupying each cage cavity, plus four more gas molecules shared between two cages in the surrounding window cavities. The smaller rare gas, krypton, is less strongly adsorbed and is much further from saturation at 1 bar (Fig. 2c, linear inset plot). The strong preference for xenon and radon adsorption is further demonstrated by calculations (Fig. 2d) that show enhanced zero-coverage heats of adsorption for xenon (31.3 kJ mol^{-1}) with respect to krypton (23.1 kJ mol^{-1}) and the more common gases that are the main constituents of air (4.5–27.7 kJ mol^{-1}). These calculations for krypton and xenon agree reasonably with measured heats of adsorption (Supplementary Information and Supplementary Fig. 1). Radon is predicted to have an even higher heat of adsorption of 38.4 kJ mol^{-1}. The computed Henry's coefficients scale with both the heats of adsorption and with the gas uptakes calculated from an equimolar 11-component competitive adsorption simulation (Fig. 2d). In this hypothetical 11-component mixture, we predict that 91.7% of the available sorption sites in the crystalline cage solid would be occupied by Rn at equilibrium, even though Rn constitutes just 9.1 mol% of the gas mixture and has a diameter, 4.17 Å, which is only 0.07 Å larger than that of Xe. These simulation data suggest selectivity for xenon and radon adsorption in this concentration range that far exceeds other reported materials[19].

Powder X-ray diffraction data were used to determine the structure of **CC3** under an excess pressure of xenon (10 bar, 295 K, Fig. 3a and Supplementary Section 2).

Single xenon atoms were located in the cage cavities and in the window cavities. At this pressure, the cage cavity is fully occupied, whereas the window cavity is 88 ± 1% occupied, resulting in a total of 2.8 xenon atoms per cage (1.87 mol kg^{-1}, 25 wt.%). A comparison can be made between this organic structure and the

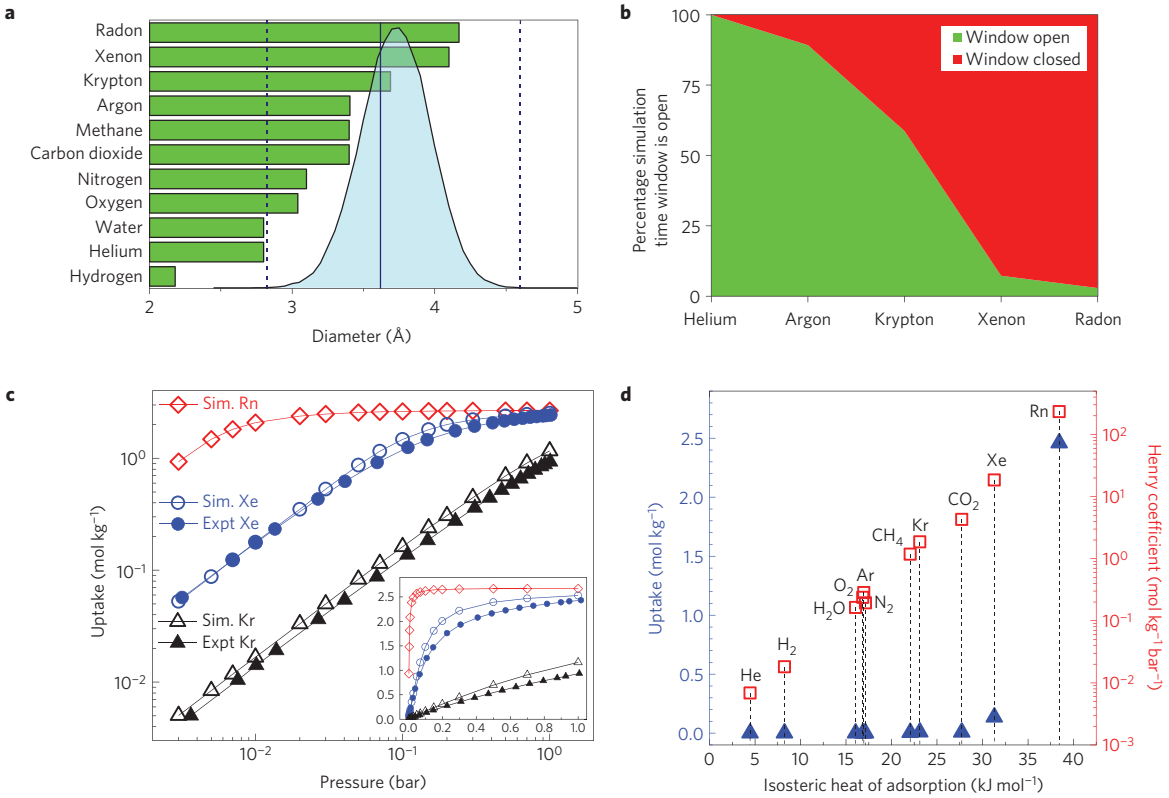

Figure 2 | Molecular simulations and adsorption measurements demonstrate dynamic gas permeability and high selectivity for xenon and radon. **a**, Molecular dynamics simulations (298 K, 1 atm) show a pore-limiting envelope (coloured blue) between 3 Å and 4.5 Å in crystalline **CC3** that encompasses the diameters of all rare gases, up to radon. The vertical dashed lines indicate the low and high limits of this pore-limiting envelope. The straight, vertical line corresponds to the pore-limiting diameter from the crystal structure. **b**, For xenon and radon, the windows are dynamically 'open' for only a small fraction of the time. **c**, Predicted single-component log–log gas adsorption isotherms (Kr, Xe and Rn; open symbols) and experimental equivalents (Kr, Xe; filled symbols) at 298 K for **CC3** (inset shows linear–linear plot). Simulated isotherms were obtained from grand-canonical Monte Carlo (GCMC) simulations. **d**, Calculated zero-coverage heats of adsorption plotted against calculated gas uptakes from a hypothetical equimolar, 11-component competitive adsorption simulations (blue triangles) and calculated Henry's coefficients (red squares), all at 298 K. We predict highly selective Rn uptake for this equimolar mixture. At equilibrium, the guest occupancy in the **CC3** pores (298 K, 1 bar total pressure) is calculated to be: Rn = 91.66%; Xe = 5.03%; Kr = 0.32%; CO_2 = 0.30%; CH_4 = 0.20%; Ar + He + N_2 + O_2 + H_2 + H_2O = 0.10%. These Henry's coefficients, supported by binary GCMC simulations, suggest that **CC3** has potential for separating various gas mixtures, in addition to the rare gases (Supplementary Section 1). Experimental adsorption data for radon are presented in the Supplementary Information (Supplementary Table 2, Supplementary Section 3.6).

known xenon hydrate (Fig. 3b; refs 23,24). At 40 K and 1.01 bar, xenon hydrate adopts a type I clathrate structure in which the polyhedral T and D-cages are 82% and 80% occupied (overall 3.87 mol kg^{-1} Xe, 51 wt.%) with average Xe–O distances of 4.26 Å and 3.86 Å, respectively. In Xe-loaded **CC3**, the closest atoms from the **CC3** molecule form analogous, polyhedral organic cages around the xenon guest (Supplementary Information and Supplementary Table 1). The shortest contact distances between the cage molecule and xenon guests are comparable to the xenon hydrate cages: the average Xe…phenyl ring centroid distance for the cage cavity is 4.22 Å, whereas short Xe…H contacts with a mean distance of 3.75 Å are present in the window cavity. The volumetric density of enclathrated xenon in **CC3** close to saturation is 0.31 g cm^{-3}. This is lower than in xenon hydrate (0.85 g cm^{-3}), but **CC3**, unlike the hydrate, is stable to removal of the xenon guest, and retains a preorganized host structure that can capture xenon at low partial gas pressures. The structure of **CC3**-*R* Kr-loaded at 9.8 bar was determined by analogous *in situ* PXRD experiments (Supplementary Section 2). This structure indicates that the krypton atoms are hosted in the cage cavity and cage window sites, with a decreased overall occupancy with respect to the xenon-loaded **CC3** structure of 2.1 ± 0.1 Kr atoms per cage (1.63 mol kg^{-1}, 13 wt.%), reflecting the much lower simulated and measured affinity of Kr for **CC3** (Fig. 2c,d).

To evaluate **CC3** for actual separations of rare gases at low concentrations in air, as would be encountered in the reprocessing of spent nuclear fuels, we carried out breakthrough measurements with an adsorption column packed with **CC3** crystals. When a mixture of xenon (400 ppm) and krypton (40 ppm) balanced with the common components of air (N_2, O_2 and CO_2) was passed through this column, the xenon component was retained for more than 15 min, even at a flow rate of 40 cm^3 STP min^{-1}, which is twice as fast as that used in previous studies for MOFs (ref. 19). By contrast, krypton and the other components broke through almost immediately (Fig. 4a).

Under these conditions, **CC3** adsorbs twice as much xenon as the leading MOF, Ni/DOBDC (ref. 19): approximately 11 mmol kg^{-1}, in good agreement with simulations (Fig. 4b). In addition, the Xe/Kr selectivity for **CC3** is almost three times higher than for Ni/DOBDC: 20.4 versus 7.3. Selectivity and capacity are often seen as a trade-off. Here, **CC3** shows significant improvements for both of these key parameters with respect to the leading MOF material[19].

These breakthrough measurements (Fig. 4a) also prove that the adsorption kinetics are fast enough to allow real separations. This is supported by kinetic studies for pure Kr and for pure Xe (Supplementary Section 3), which show that rare gas diffusion in **CC3** is relatively fast (for example, at 2.0 mbar, 195 K; Kr = 12.7 × 10^{-3} s^{-1} and Xe = 5.76 × 10^{-3} s^{-1}). Comparison of activation energies, E_a, with the corresponding enthalpies of adsorption, Q_{st}, for Kr and Xe

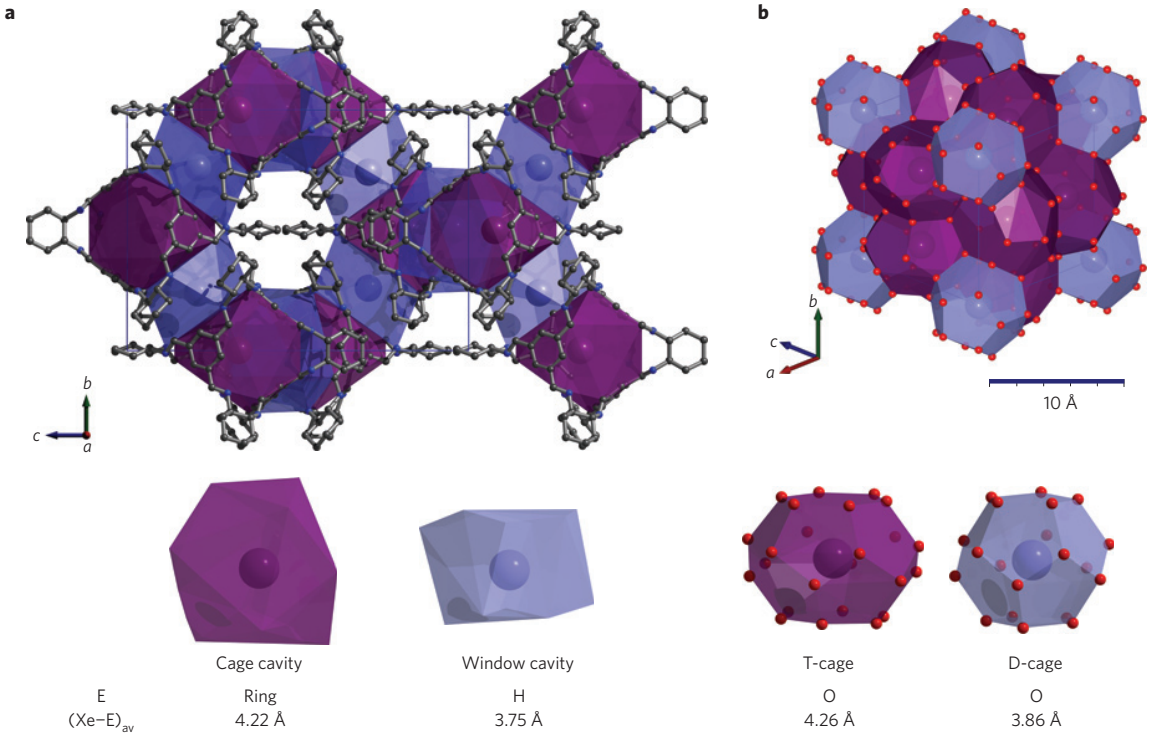

Figure 3 | Gas-loaded organic cage structures have parallels with gas hydrates. a,**b**, Structural comparison between porous organic xenon clathrate (**a**) and xenon hydrate, (**b**). The sizes of the organic cage cavities (dark purple) and the inter-window cavities (light purple) in the pre-structured, porous organic clathrate are analogous to the D- and T-cages in the ice hydrate. In both cases, a single xenon atom occupies each cavity. $(Xe–E)_{av}$ is the average distance between xenon and its neighbouring element or ring centroid (E) in each structure.

show that E_a is lower than Q_{st}. The Xe and Kr adsorption kinetics at 195 K show that a surface barrier is involved in the rate-controlling step for adsorption of both gases on **CC3**.

We ascribe the dramatic separation performance to the near-perfect fit between the cavities in **CC3** and the xenon guests. Indeed, the pore structure in **CC3** reflects the optimal, hypothetical structure for Xe/Kr separation suggested by computational studies[18]: that is, uniform pore channels that are at points too narrow, but at other points just large enough, to accommodate a single xenon atom. There are no larger cavities in **CC3** that are a poor fit for xenon, nor any smaller cavities that might competitively adsorb the smaller molecules, such as nitrogen or water, in the gas mixture. Other molecular host–guest complexes[25,26] and organic clathrates[27] of the rare gases have been formed, but in the presence of much higher rare gas concentrations, often in solution, under conditions that would be impractical for selective gas capture from dilute mixtures with air.

The organic cage is also an excellent adsorbent for radon gas. Although metal–organic frameworks have been studied recently for radon separation by molecular modelling[28,29], they have not yet been subject to any experimental tests. The adsorption capacity for **CC3** was evaluated by a dynamic adsorption technique where the radioisotope is mixed at high dilution in a carrier gas, nitrogen. The radon concentration in the gas was $615 \pm 17\ Bq\ m^{-3}$, or $3.8 \pm 0.1 \times 10^{-16}\ mol\ kg^{-1}$. The cage crystal adsorbs ^{222}Rn from the gas phase and concentrates it in the solid state by a volumetric factor of between 5,000 and 1×10^6, depending on the adsorption temperature (Supplementary Information and Supplementary Table 2). This high selectivity for radon with respect to nitrogen was also predicted at ambient temperature for multicomponent air (Fig. 4c), which includes potentially competing species such as CO_2 and water. Hence, **CC3** might be useful for radon removal from air, or from water, or for improving the sensitivity and humidity tolerance of environmental monitoring technologies that use physical adsorption to concentrate the radon gas for detection. At present, charcoal is used as an adsorbent for short-term radon testing in domestic homes, but its relatively poor selectivity against water vapour can lead to variation in test results with fluctuating humidity. In principle, **CC3**, which has a single pore size that is tailored to adsorb radon, offers a solution to this problem.

Experiments with radioisotopes are restricted to specialized laboratories, but radioisotope adsorption is readily studied *in silico*. For example, we also predict that **CC3** could capture ^{222}Rn from helium at radon concentrations as low as 0.01 ppmv (Supplementary Information and Supplementary Fig. 2) with extremely high selectivity ($Rn/He = 5.4 \times 10^8$), as relevant in astroparticle physics experiments searching for rare, low-energy events[30]. Our success in calculating the Xe and Kr behaviour relative to experimental results (Fig. 4b) gives us confidence in extrapolating these computational predictions to radon.

This porous organic cage can also be used to separate molecules other than rare gases. Chiral molecules are important pharmaceutical feedstocks and there is a need for their effective separation[31]. **CC3** can be prepared in homochiral form by synthesizing the cage from either the (*R*,*R*) or (*S*,*S*) enantiomer of 1,2-cyclohexanediamine[32]. We therefore explored homochiral **CC3** for chiral separations that are important, for example, in the pharmaceutical industry[31]. Homochiral crystals of **CC3** were found to adsorb a chiral alcohol, 1-phenylethanol, with selectivity for the enantiomer with opposite chirality to that of the cage (Fig. 5a and Supplementary Section 4). This results from more favourable intermolecular interactions between the 1-phenylethanol guest and the **CC3** cage of the opposite chirality. Neither the solid racemic cage crystal, *rac*-**CC3**, nor a chiral conglomerate of **CC3**, showed any enantioselectivity for this alcohol. However, *rac*-**CC3** does show size selectivity for achiral guests, such as xenon and radon, much as found for the homochiral forms of **CC3**. Hence, *rac*-**CC3** is size selective, whereas homochiral **CC3** is both size selective and enantioselective.

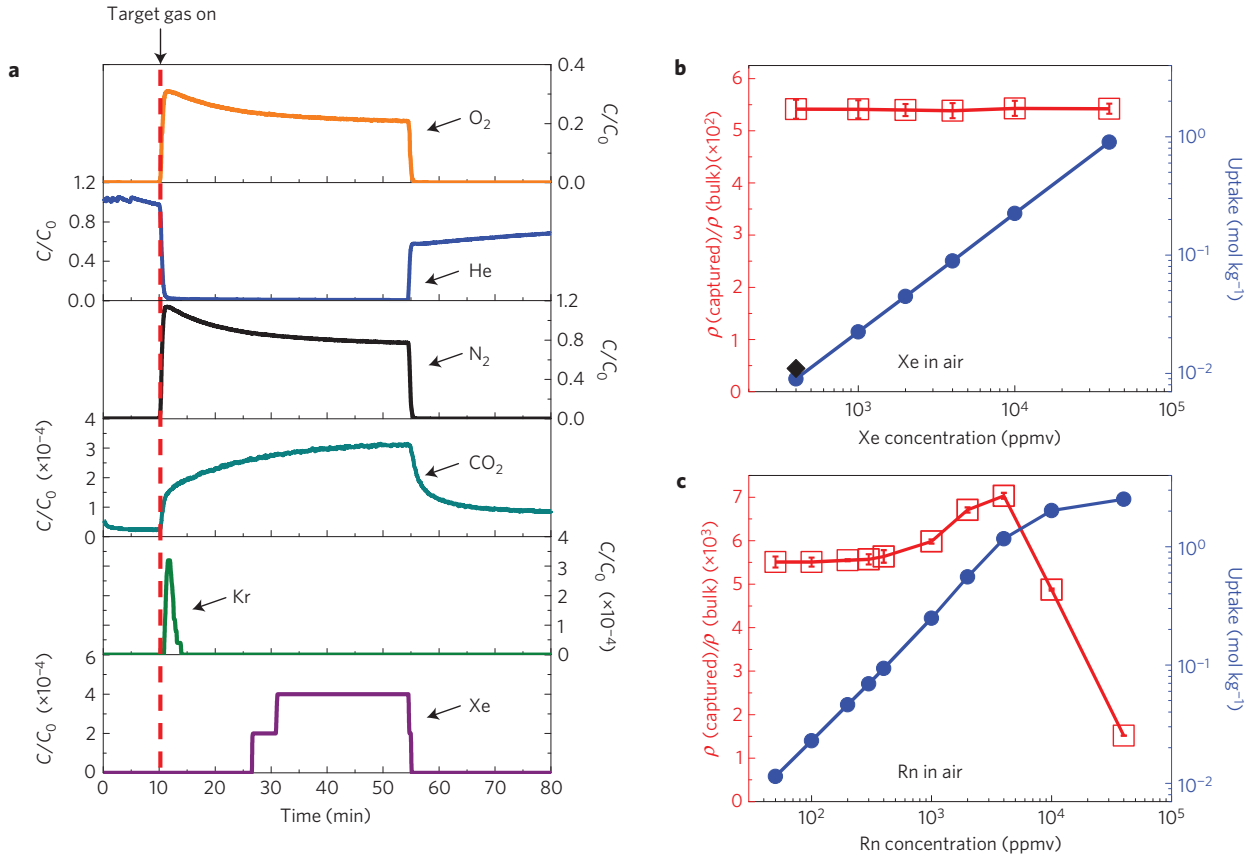

Figure 4 | Separation of valuable or harmful rare gases at low concentrations using organic cages. a, Breakthrough measurements show clean separation of krypton (40 ppm) from xenon (400 ppm) when present as low-concentration impurities diluted in air, as might be encountered in nuclear reprocessing technologies ($T = 298$ K; C, concentration of component in column outlet; C_0, total concentration of all feed gases). **b**, The experimental xenon uptake (400 ppm Xe) is also reproduced by simulations; black diamond, experimental uptake. The volumetric density of the rare gas in the solid **CC3** adsorbent divided by its volumetric density in the bulk gas phase, ρ (captured)/ρ (bulk) (left vertical axis), is plotted against its concentration in the gas mixture (red squares), together with the corresponding simulated rare gas uptake (blue circles, right vertical axis). **c**, Other simulations, also at 298 K, predict even higher selectivity for radon separation from air, or from pure nitrogen or helium (Supplementary Information and Supplementary Fig. 2), as validated by gas adsorption experiments.

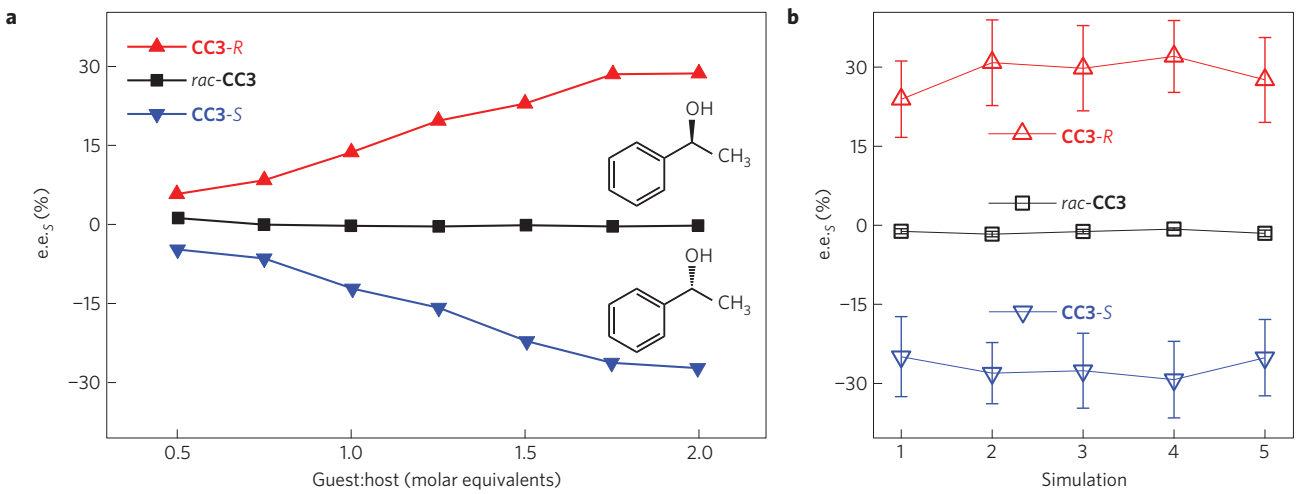

Figure 5 | Chiral separation using CC3. a, Measured enantiomeric excess of the *S* enantiomer (e.e.$_S$) of 1-phenylethanol adsorbed in **CC3** over a range of guest:host ratios. Equal and opposite e.e.$_S$ is observed for homochiral **CC3**-*R* (red) and **CC3**-*S* (blue) crystals because of preferential adsorption of the 1-phenylethanol enantiomer with opposite chirality. The racemic cage crystal, *rac*-**CC3** (black), is not enantioselective. **b**, Simulated e.e.$_S$ obtained from advanced configurational-bias Monte Carlo simulations for 1-phenylethanol in the **CC3** host. All simulations were carried out at ambient temperature and pressure. Simulated maximum guest loadings and e.e.$_S$ for 1-phenylethanol in the **CC3** host correspond closely with experimental observations at a guest:host ratio of 2. Five independent simulations were performed in each case.

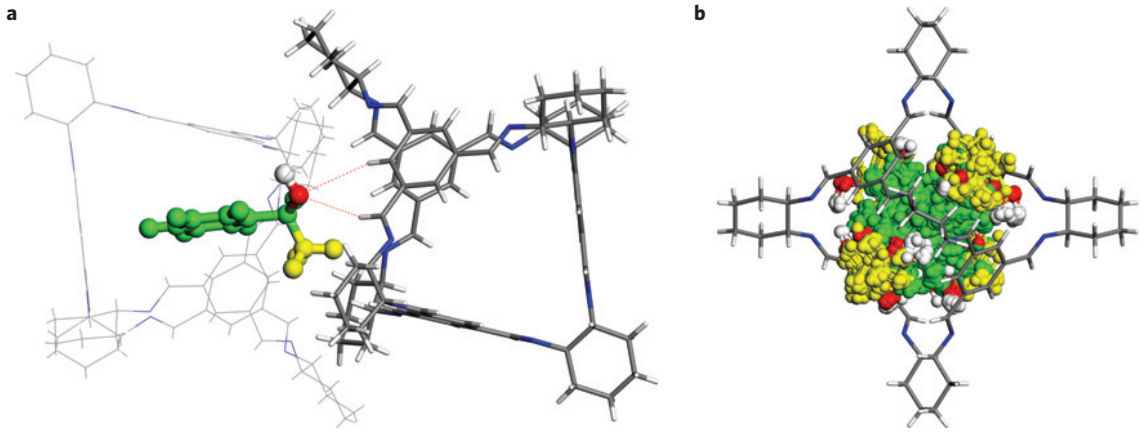

Figure 6 | Simulated molecular configurations of (*S*)-1-phenylethanol in the pores of CC3-*R*. a, A frequently observed conformation where the hydroxyl oxygen atom of (*S*)-1-phenylethanol (red) is in close proximity to the hydrogen atom (2.57 Å), bonded to an imine carbon atom, and to an aryl hydrogen atom (2.61 Å), both of **CC3**-*R*. **b**, Overlay of one hundred snapshots of (*S*)-1-phenylethanol in the **CC3**-*R* cage molecule. The alcohol groups (red, O; white, H) and the methyl groups (yellow) of (*S*)-1-phenylethanol occupy the cage windows, pointing towards neighbouring cages; the phenyl ring (green) is located inside the cage cavity. The predicted disordered orientation of (*S*)-1-phenylethanol inside the **CC3**-*R* cage is consistent with experimental single-crystal observations.

As for the size-selective binding of rare gases, molecular simulations can predict the observed enantioselectivity in **CC3**. A parallel mole-fraction grand-canonical Monte-Carlo simulation[33] was used to predict the enantiomeric excess of 1-phenylethanol in **CC3**, and the results show close agreement with experiment (Fig. 5b). Single-crystal X-ray diffraction shows that the 1-phenylethanol guests are disordered over several sites in the pores of **CC3** (Supplementary Section 4). The electron density is too diffuse to be modelled accurately, but molecular simulations suggest that the chiral selectivity stems from a specific interaction between the hydroxyl group in the alcohol and the nitrogen atom in the imine of **CC3** (Fig. 6a), supported by π–π interactions between aryl groups in the cage and in the alcohol. This conformation is predicted to be common for (*S*)-1-phenylethanol in **CC3**-*R*, but is much less apparent in **CC3**-*S*, as illustrated by radial distribution function plots (Supplementary Information and Supplementary Figs 3–5). This leads to a predicted difference in host–guest binding energy for (*S*)-1-phenylethanol and (*R*)-1-phenylethanol in **CC3**-*R* of approximately $28.5 \pm 4.0\,\mathrm{kJ\,mol^{-1}}$, which explains the observed enantioselectivity. As for the radon gas studies above (Fig. 2c), molecular simulations provide details that are not readily obtained by experiment[34], in this case because of the disorder of the guest in the host pore channels.

These results suggest that porous organic cage solids have potential for analytical chiral separations, or perhaps even preparative separations given the scalability and hydrothermal stability of **CC3** (ref. 35) and its derivatives[36]. Chiral selectivity is known for porous MOFs (refs 37–40), metal–organic cages[41] and, recently, hydrogen bonded organic frameworks[42]. Porous organic cage materials, however, might have specific advantages. In particular, unlike extended frameworks, they can be highly soluble in organic solvents[43], and this could allow direct solution deposition in practical formats such as capillary columns, thus avoiding problems that can be encountered with slurries of insoluble porous frameworks[40]. Indeed, solution processing of organic cages has already been used to produce hierarchically porous solids[44] and materials for molecular sensing[45].

In summary, porous organic cages have unprecedented selectivity for rare gas separations at low rare gas concentrations. These porous molecules also show promise for chiral separations. The underlying principles of size-selective and enantioselective binding, supported by molecular simulations, could be extended to larger guests, such as biomolecules, by exploiting, for example, the larger, mesoporous cage molecules that have been discovered recently[46–49].

Received 14 November 2013; accepted 16 June 2014; published online 20 July 2014

References

1. Kerry, F. G. *Industrial Gas Handbook: Gas Separation and Purification* (CRC Press, 2007).
2. Darby, S. *et al.* Radon in homes and risk of lung cancer: Collaborative analysis of individual data from 13 European case-control studies. *Br. Med. J.* **330,** 223–227 (2005).
3. Turkevich, A., Winsberg, L., Flotow, H. & Adams, R. M. The radioactivity of atmospheric krypton in 1949–1950. *Proc. Natl Acad. Sci. USA* **94,** 7807–7810 (1997).
4. Bowyer, T. W. *et al.* Elevated radioxenon detected remotely following the Fukushima nuclear accident. *J. Environ. Radioact.* **102,** 681–687 (2011).
5. Rutherford, E. Absorption of the radio-active emanations by charcoal. *Nature* **74,** 634 (1906).
6. Munakata, K. *et al.* Adsorption equilibria of krypton, xenon, nitrogen and their mixtures on molecular sieve 5 Å and activated charcoal. *J. Nucl. Sci. Technol.* **36,** 818–829 (1999).
7. Gaul, W. C. & Underhill, D. W. Dynamic adsorption of radon by activated carbon. *Health Phys.* **88,** 371–378 (2005).
8. Wright, P. A. *Microporous Framework Solids* (Royal Society of Chemistry, 2008).
9. Li, J. R., Kuppler, R. J. & Zhou, H. C. Selective gas adsorption and separation in metal–organic frameworks. *Chem. Soc. Rev.* **38,** 1477–1504 (2009).
10. Bloch, E. D. *et al.* Hydrocarbon separations in a metal–organic framework with open iron(II) coordination sites. *Science* **335,** 1606–1610 (2012).
11. Couderc, G. *et al.* Reversible sorption of nitrogen and xenon gas by the guest-free zeolite tris(*o*-phenylenedioxy)cyclotriphosphazene (TPP). *Micropor. Mesopor. Mater.* **88,** 170–175 (2006).
12. Carta, M. *et al.* An efficient polymer molecular sieve for membrane gas separations. *Science* **339,** 303–307 (2013).
13. Van Heest, T. *et al.* Identification of metal–organic framework materials for adsorption separation of rare gases: Applicability of ideal adsorbed solution theory (IAST) and effects of inaccessible framework regions. *J. Phys. Chem. C* **116,** 13183–13195 (2012).
14. Mitra, T. *et al.* Molecular shape sorting using molecular organic cages. *Nature Chem.* **5,** 276–281 (2013).
15. Bae, Y. S. *et al.* High xenon/krypton selectivity in a metal–organic framework with small pores and strong adsorption sites. *Micropor. Mesopor. Mater.* **169,** 176–179 (2013).
16. Wang, H. *et al.* The first example of commensurate adsorption of atomic gas in a MOF and effective separation of xenon from other noble gases. *Chem. Sci.* **5,** 620–624 (2014).
17. Liu, J., Strachan, D. M. & Thallapally, P. K. Enhanced noble gas adsorption in Ag@MOF-74Ni. *Chem. Commun.* **50,** 466–468 (2014).

18. Sikora, B. J., Wilmer, C. E., Greenfield, M. L. & Snurr, R. Q. Thermodynamic analysis of Xe/Kr selectivity in over 137 000 hypothetical metal–organic frameworks. *Chem. Sci.* **3,** 2217–2223 (2012).
19. Liu, J., Thallapally, P. K. & Strachan, D. Metal–organic frameworks for removal of Xe and Kr from nuclear fuel reprocessing plants. *Langmuir* **28,** 11584–11589 (2012).
20. Tozawa, T. *et al.* Porous organic cages. *Nature Mater.* **8,** 973–978 (2009).
21. Willems, T. F. *et al.* Algorithms and tools for high-throughput geometry-based analysis of crystalline porous materials. *Micropor. Mesopor. Mater.* **149,** 134–141 (2012).
22. Haldoupis, E., Nair, S. & Sholl, D. S. Pore size analysis of >250,000 hypothetical zeolites. *Phys. Chem. Chem. Phys.* **13,** 5053–5060 (2011).
23. Yang, L. *et al.* Synthesis and characterization of a new structure of gas hydrate. *Proc. Natl Acad. Sci. USA* **106,** 6060–6064 (2009).
24. Ohgaki, K., Sugahara, T., Suzuki, M. & Jindai, H. Phase behavior of xenon hydrate system. *Fluid Phase Equilib.* **175,** 1–6 (2000).
25. Fogarty, H. A. *et al.* A cryptophane core optimized for xenon encapsulation. *J. Am. Chem. Soc.* **129,** 10332–10333 (2007).
26. Fairchild, R. M. *et al.* A water-soluble Xe@cryptophane-111 complex exhibits very high thermodynamic stability and a peculiar ^{129}Xe NMR chemical shift. *J. Am. Chem. Soc.* **132,** 15505–15507 (2010).
27. Taratula, O. *et al.* Crystallographic observation of 'induced fit' in a cryptophane host–guest model system. *Nature Commun.* **1,** 148 (2010).
28. Parkes, M. V. *et al.* Screening metal–organic frameworks for selective noble gas adsorption in air: Effect of pore size and framework topology. *Phys. Chem. Chem. Phys.* **15,** 9093–9106 (2013).
29. Perry, J. J. *et al.* Noble gas adsorption in metal–organic frameworks containing open metal sites. *J. Phys. Chem. C* **118,** 11685–11698 (2014).
30. Simgen, H. Radon assay and purification techniques. *AIP Conf. Proc.* **1549,** 102–107 (2013).
31. Lorenz, H. & Seidel-Morgenstern, A. Processes to separate enantiomers. *Angew. Chem. Int. Ed.* **53,** 1218–1250 (2014).
32. Hasell, T. *et al.* Porous organic cage nanocrystals by solution mixing. *J. Am. Chem. Soc.* **134,** 588–598 (2012).
33. Dubbeldam, D., Torres-Knoop, A. & Walton, K. S. On the inner workings of Monte Carlo codes. *Mol. Simul.* **39,** 1253–1292 (2013).
34. Dubbeldam, D., Calero, S. & Vlugt, T. J. H. Exploring new methods and materials for enantioselective separations and catalysis. *Mol. Simul.* **40,** 585–598 (2014).
35. Hasell, T. *et al.* Reversible water uptake by a stable imine-based porous organic cage. *Chem. Commun.* **48,** 4689–4691 (2012).
36. Liu, M. *et al.* Acid- and base-stable porous organic cages: Shape persistence and pH stability via post-synthetic 'tying' of a flexible amine cage. *J. Am. Chem. Soc.* **136,** 7583–7586 (2014).
37. Seo, J. S. *et al.* A homochiral metal–organic porous material for enantioselective separation and catalysis. *Nature* **404,** 982–986 (2000).
38. Kim, K., Banerjee, M., Yoon, M. & Das, S. Chiral metal–organic porous materials: Synthetic strategies and applications in chiral separation and catalysis. *Top. Curr. Chem.* **293,** 115–153 (2010).
39. Dybtsev, D. N. *et al.* A homochiral metal–organic material with permanent porosity, enantioselective sorption properties, and catalytic activity. *Angew. Chem. Int. Ed.* **45,** 916–920 (2006).
40. Liu, B. Metal–organic framework-based devices: Separation and sensors. *J. Mater. Chem.* **22,** 10094–10101 (2012).
41. Xuan, W. *et al.* A chiral quadruple-stranded helicate cage for enantioselective recognition and separation. *J. Am. Chem. Soc.* **134,** 6904–6907 (2012).
42. Li, P. *et al.* A homochiral microporous hydrogen-bonded organic framework for highly enantioselective separation of secondary alcohols. *J. Am. Chem. Soc.* **136,** 547–549 (2014).
43. Hasell, T. *et al.* Controlling the crystallization of porous organic cages: Molecular analogs of isoreticular frameworks using shape-specific directing solvents. *J. Am. Chem. Soc.* **136,** 1438–1448 (2014).
44. Hasell, T., Zhang, H. & Cooper, A. I. Solution-processable molecular cage micropores for hierarchically porous materials. *Adv. Mater.* **24,** 5732–5737 (2012).
45. Brutschy, M., Schneider, M. W., Mastalerz, M. & Waldvogel, S. R. Porous organic cage compounds as highly potent affinity materials for sensing by quartz crystal microbalances. *Adv. Mater.* **24,** 6049–6052 (2012).
46. Mastalerz, M., Schneider, M. W., Oppel, I. M. & Presly, O. A salicylbisimine cage compound with high surface area and selective CO_2/CH_4 adsorption. *Angew. Chem. Int. Ed.* **50,** 1046–1051 (2011).
47. Mastalerz, M. Shape-persistent organic cage compounds by dynamic covalent bond formation. *Angew. Chem. Int. Ed.* **49,** 5042–5053 (2010).
48. Zhang, G. *et al.* A permanent mesoporous organic cage with an exceptionally high surface area. *Angew. Chem. Int. Ed.* **53,** 1516–1520 (2014).
49. Zhang, G. *et al.* A shape-persistent quadruply interlocked giant cage catenane with two distinct pores in the solid state. *Angew. Chem. Int. Ed.* **53,** 5126–5130 (2014).

Acknowledgements

We thank EPSRC (EP/H000925/1; EP/K018396/1), the European Research Council under FP7 (ERC grant agreement no. 321156) and Region PACA (Provence-Alpes-Cote-d'Azur) for funding. A.I.C. is a Royal Society Wolfson Merit Award holder. K.E.J. is a Royal Society University Research Fellow. We thank Diamond Light Source for access to beamlines I11 (EE7040) and I19 (MT8728) that contributed to the results presented here. We also thank the beamline staff for their assistance during the I11 experiments. We thank D. Dubbeldam for providing the RASPA simulation package. We thank the US Department of Energy (DOE), Office of Nuclear Energy, and in particular, J. Bresee, for their support. T. Todd (Idaho National Laboratory) and B. Jubin (Oak Ridge National Laboratory) provided programmatic support and guidance. Pacific Northwest National Laboratory is a multiprogram national laboratory operated for the US Department of Energy by Battelle Memorial Institute under Contract DE-AC05-76RL01830.

Author contributions

L.C., D.H. and K.E.J. performed the molecular simulations. P.S.R., J.L., D.M.S. and P.K.T. conceived and carried out the gas breakthrough measurements. S.Y.C. and M.A.L. carried out X-ray structure analyses. T.H., K.M.T., J.A.A. and J. Bell performed gas sorption analyses. R.N. and J. Busto carried out the radon adsorption measurements. A.K., M.E.B. and A.S. determined chiral selectivities. A.K., A.S., M.A.L., M.E.B., P.S.R., S.Y.C., and T.H. prepared the cage molecules. A.I.C. conceived the project. All coauthors contributed to the writing of the paper.

Additional information

Supplementary information is available in the online version of the paper. Reprints and permissions information is available online at www.nature.com/reprints. Correspondence and requests for materials should be addressed to A.I.C.

Competing financial interests

The authors declare no competing financial interests.